USING ELECTRONIC NAVIGATIONAL CHART FOR 3D BATHYMETRIC MODEL OF THE PORT OF NAPLES

Emanuele Alcaras, Pier Paolo Amoroso, Francesco G. Figliomeni, Claudio Parente, and Andrea Vallario

Dept of Science and Technology, Parthenope University of Naples, Italy

Commission IV, WG 7

KEY WORDS: 3D bathymetric model, GIS, ENC, interpolation, deterministic methods, stochastic methods, Kriging.

ABSTRACT:

Nautical charts generally report fundamental knowledge for the safety of navigation. This information also includes sea depth data reported as depth points or contour lines, which can be used to build a 3D model of the seabed. However, there are different interpolation methods for creating digital depth models, and there is no way to know in advance which of them is the best performing. The aim of this work is to compare different spatial interpolation methods applied on a dataset concerning the seabed of the Port of Naples (Italy) and extracted from the Electronic Navigational Chart (ENC) produced by the Hydrographic Institute of the Italian Navy, in scale 1:10.000. Four deterministic interpolation methods, i.e. Inverse Distance Weighting (IDW), Global Polynomial Interpolation (GPI), Local Polynomial Interpolation (LPI), Radial Basis Function (RBF), and two stochastic interpolation methods, i.e. Ordinary Kriging (OK) and Universal Kriging (UK), are applied using Geographic Information System (GIS) software. Since each method requires to set specific parameters and different options are available, e.g. the order of the polynomial function for GPI and LPI, or semi-variograms for OK and UK, twenty-three models are generated. The result quality is evaluated by Leave-One-Out cross-validation and the statistics of the residuals produced by each interpolation method in the measured points are compared and analysed. The experiments confirm that the stochastic approach is more versatile compared to deterministic approach and can produce better results, as it is testified by the great performance of the Ordinary Kriging, which produces the most accurate 3D models.

1. INTRODUCTION

The ocean floor is the last great, largely un-surveyed area of Earth (Hare et al., 2011). The study of the underwater depth of ocean, sea, lake or river floor is referred as bathymetry (Weatherall et al.., 2015) and it can be carried out for various purposes, such as shipwrecks identification (Plets et al., 2015), monitoring of the effects of natural disasters (Frederik et al.., 2019), geophysical purposes (Ladage et al.., 2006), estimation of the upper depth limit of seagrasses (Infantes et al., 2009), safety of navigation (Kristić et al., 2020). Bathymetric surveys based on single beam and multibeam echosounders allow to acquire depth data of a given area (Dabrowski et al., 2021).

The maps used for navigation, namely nautical charts, present distinctive elements for the knowledge of the seabed such as contour lines (called depth contours or isobaths) and selected depths (soundings) (Alcaras et al., 2021). As well known, a contour line is a curve that joins points of equal value; in cartography, contour lines join the points of equal elevation above a given standard reference surface like the mean sea level. Specifically, charted depths displayed on nautical charts are measured from the level of water derived from some phase of the tide. The reference level is named Chart datum and commonly identified as the lowest astronomical tide (LAT), used for example in United Kingdom, Canada and Australia, or the mean lower low water (MLLW), used in USA and Italy. Chart Datum is shown on charts as the zero-metre contour.

Nautical charts are manageable by information systems that support navigation, i.e. Electronic Charting Systems (ECS) and Electronic Chart Display and Information Systems (ECDIS) (Brčić et al., 2015). Nautical charts in vector format that comply with specific standards dictated by the International Hydrographic Organization (IHO), are called electronic navigation charts (ENCs) (Alcaras et al., 2021) and its use is mandatory for ECDIS. ENC is a major source of information for the navigator and for the safety of navigation, as it provides information on the depth of an area (Wlodarczyk-Sielicka and Stateczny, 2016).

Since soundings and contour lines included in the ENC supply depth (z) variability related to planimetric position (x, y), it is possible to use those data to generate 3D models of the seabed. Even if the depth data usable for 3d modelling can be acquired with direct on-site survey techniques such as single beam and multibeam, ENCs are the most easily available and also the cheapest source of information. In general, a 3D model of the Earth's surface is called Digital Terrain Model (DTM) and it is often structured as a grid presenting height value in each node, so to result as a matrix of numbers (Digital Elevation Model, DEM); particularly a 3D model of the seabed is called Digital Depth Model (DDM) (Parente, Vallario, 2019).

A 3D grid model can be generated using an interpolation method that estimates the value of elevation or depth in each node starting from the known elevations or depths of neighbouring points. In literature there are several interpolation methods to build a 3D grid model (Arun, 2013); however, there is no way of knowing a priori which of them is the best for a given dataset.

This work aims to analyse interpolation methods capable of generating DDMs and compare them to determine the most performing one, in relation to a dataset of depth points and contour lines extracted from the ENC of the Port of Naples in scale 1:10,000.

This paper is organized as follows. Section 2 focuses on the study area and dataset. Section 3 describes: firstly, the main characteristics of the interpolation methods adopted for DDM construction; then the analysis process for each model accuracy evaluation. Section 4 introduces and discusses the results obtained from the application of the selected methods. Finally, Section 5 draws out the conclusions of this research study and highlights areas for future work.

2. STUDY AREA AND DATASET

The area considered for this study concerns the Port of Naples (Italy) and surroundings, as shown in Figure 1. The Port of Naples is one of the most important ports in Europe; it occupies the northernmost natural inlet of the Gulf of Naples and extends for about 12 km, from the city centre towards its eastern part. The total area extends for over 4.086 sq. km and is utilized for multifunctional use for a total of 14 piers.

Depth data for this work are obtained from the ENC n. 84 produced by Hydrographic Institute of the Italian Navy (Istituto Idrografico della Marina Militare Italiana – IIMM), in scale 1:10,000. The original file is formed in accordance with the standards established by the International Hydrographic Organization (S-57 IHO), so we convert it as shape format (.shp) for using in ArcGIS version 10.8 (ESRI). However, several files are produced, one for each layer included in the ENC. Firstly, we transform the reference system from WGS84 ellipsoidal coordinates (EPSG code: 4326) in the Universal Transverse of Mercator (UTM) - WGS84 - Zone 33 N (EPSG code: 32633), then we select only the depth data that are included in two layers named contour lines (depths in meters: 0, -2, -5, -10, -20, -30, -50, -100) and soundings (from -1.30 m to -128.00 m); finally, we group the vertices of contour lines and the soundings in one shape file.

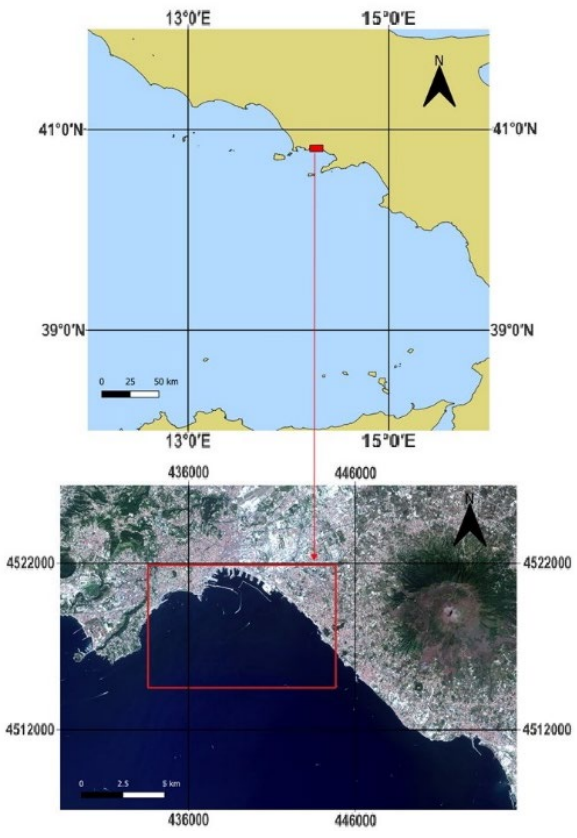

Figure 1. Geo-localization of the Port of Naples: map in equirectangular projection and WGS 84 geographic coordinates (upper); RGB composition of Sentinel-2 images in UTM-WGS84 - Zone 33 N - plane coordinates expressed in meters (lower).

As shown in Figure 2, the resulting dataset extends within the following UTM/WGS84 plane coordinates – 33T zone: E_1= 433,621 m, E_2= 444,624 m, N_1= 4,514,622 m, N_2= 4,521,768 m. It includes 16,853 points and depth values range between 0 m and -128 m.

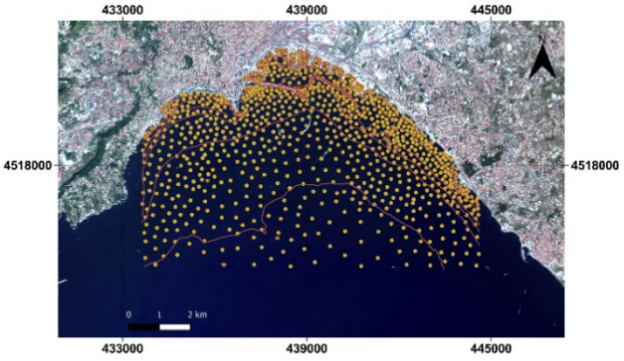

Figure 2. The point dataset extracted from the ENC n. 84 concerning the Port of Naples and used for Digital Depth Models (UTM-WGS84 - Zone 33 N plane coordinates expressed in meters).

3. METHODS

Spatial interpolation is a very important component of many Geographical Information Systems (GIS) and we can define it as the procedure to predict the value of attributes at unobserved points within a study area covered by existing observations (Krivoruchko, 2011).

Spatial interpolation methods can be divides in two main categories: global and local. Global methods use all available data in the region of interest to derive the estimation and capture the general trend; local methods operate within a small area around the point being estimated, using samples in a search window, and capture the local or short-range variations (Li, Heap, 2019).

Another way to classify these methods is to differentiate them into deterministic and stochastic. Deterministic methods use point values directly, while stochastic methods incorporate the concept of randomness and use statistical techniques to analyse the data and statistical criteria for predictions (Mitas, Mitasova, 1999). In other words, the deterministic methods use mathematical functions to predict unknown values, while geostatistical methods use statistics and mathematical functions as well (Ajvazi, Czimber, 2019).

Another distinction can be made in exact and approximate. Exact interpolators do match the measured values on which the interpolation is based; thus, the predicted surface must pass through each measured data point. Approximate interpolators utilize the measured values in calculating the predicted surface, but the surface is not restricted to passing through the measured values at those locations (Eberly get al., 2004).

In this study, we consider four deterministic methods, i.e. Inverse Distance Weight (IDW), Global Polynomial Interpolation (GPI), Local Polynomial Interpolation (LPI), Radial Basis Function (RBF), and two stochastic interpolation methods, i.e. Ordinary Kriging (OK) and Universal Kriging

(UK), all available in Geostatistical Analyst, an extension of ArcGIS Software. For OK and UK different semi-variogram models are used, such as Stable (S), J-Bessel (JBS), K-Bessel (KBS), Exponential (ES).

Semi-variogram is a diagram in which the semi-variance is represented as a function of the distance between two points (Zimmerman and Zimmerman, 1991). The semi-variance function is given by the formula (Walvoort, de Gruijter, 2001):

$$\gamma(h) = \frac{1}{2n}\sum_{i=1}^{n}(z(x_i) - z(x_i + h))^2 \quad (1)$$

where: γ(h) is the value of the semi-variance at the distance d;
n is the number of couples of points separated by *h*;
z is the value of the depth;
x_i and x_i+h indicate the positions of each couple of points.

3.1 Inverse Distance Weighting (IDW)

IDW is largely used in various fields such as earth sciences, hydrology and environmental sciences (Koutroulis et al., 2011). IDW makes the assumption that things close to one another are more similar than those are far. The attributed values to unknown points are calculated with a weighted average between available known points.

The interpolation function can be written as:

$$Z_{x,y} = \frac{\sum_{k=1}^{N}\frac{Z_k}{d_k^p}}{\frac{1}{d_k^p}} \quad (2)$$

where $Z_{x,y}$ = estimated value at the position (x, y) of the grid;
z_k = a neighbouring data point value;
N = the number of neighbouring points;
d_k = the distance between the data point and the point being interpolated;
P = a positive-power parameter.

In other terms, to predict a value for any not measured location, IDW uses the measured values available. IDW assumes that each measured point has a greater influence that decreases with distance, hence the name inverse distance weighting. This weight is modulated by the power. In this study, IDW with power equal to 2 is applied.

3.2 Global polynomial interpolation (GPI)

Global polynomial interpolation (GPI) fits a smooth surface that is defined by a mathematical function (a polynomial) to the input sample points. The result from global polynomial interpolation is a smooth surface that represents gradual trends in the surface over the area of interest (Johnston et al., 2001).
The interpolation function can be written as (Parente and Vallario, 2019):

$$z = \sum_{i=0}^{m_1}\sum_{j=0}^{m_2} a_{i,j}x^i y^i \quad (3)$$

Where, if n is the order of the equation:

$0 \le m_1 \le n$;
$0 \le m_2 \le n$;
$m_1 + m_2 \le n$;
$a_{i,j}$ are determined using the known values in the sample points.

GPI obtains predictions using the entire dataset instead of using the measured points within neighbourhoods. GPI 1st order (GPI-1) fits a flat plane; GPI 2nd order (GPI-2) fits a surface with one bend, GPI 3rd order (GPI-3) fits a surface with two bends, and so forth (Wang et al., 2014).

3.3 Local polynomial interpolation (LPI)

Local polynomial interpolation fits the specified order (zero, first, second, third, and so on) polynomial using points only within the defined neighbourhood. The neighbourhoods overlap, and the value used for each prediction is the value of the fitted polynomial at the centre of the neighbourhood (Johnston et al., 2001).

Local polynomial interpolation uses a local subset defined by a window (Luo et al., 2008). This window is shifted across the map area and the surface value at the centre of the window is estimated. Naturally, the size of the window must be large enough to include a correct number of data points (De Smith et al., 2007).

3.4 Radial Basis Function (RBF)

Radial basis function methods are modern ways to approximate multivariate functions, especially in the absence of grid data (Baxter, 2010). A radial basis function approximation takes the form:

$$s(x) = \sum_{i\in I} y_i \varphi(\|x - i\|), \qquad x \in R^d \quad (4)$$

where φ:[0, ∞) → R is a fixed univariate function and the coefficients $(y_i)_{i\in I}$ are real numbers;
$\|x - i\|$ represents the norm, and the Euclidean norm is the most common choice;
S is represented as a linear combination of translations of a fixed function that is radially symmetric with respect to the given norm (Buhmann, 2009).

In this study we apply different basis functions such as: completely regularized spline RBF-CRS, spline with tension RBF-SWT, thin-plate spline RBF-TPS, multiquadric function RBF-MF, inverse multiquadric function RBF-IMF. Each basis function generates a different interpolation surface (Johnston et al., 2001).

3.5 Ordinary Kriging (OK)

OK is one of the most commonly used Kriging techniques (Setianto and Triandini, 2013). Its aim is to predict the value of the random variable $z(x_0)$ at an unsampled point x_0 of a geographical region as well (Webster, Oliver, 2007).
It assumes the model:

$$z(x_0) = \sum_{i=1}^{n}\lambda_i z(x_i) \quad (5)$$

Where: λ_i are the kriging weights.

The function $z(x_i)$ is composed of a deterministic component μ and a random function $\varepsilon(x_i)$ (Oliver et al., 1989).

$$z(x_i) = \mu + \varepsilon(x_i) \quad (6)$$

The deterministic component is a constant value for each x_i location in each area.
In this study, we analyse this method varying the models of the semi-variogram.

3.6 Universal Kriging (UK)

UK assumes the model (Johnston et al., 2001):

$$z(x_i) = \mu(x_i) + \varepsilon(x_i) \quad (7)$$

where, $z(x_i)$ is the variable of interest, $\mu(x_i)$ is some deterministic function and $\varepsilon(x_i)$ is random variation (Gundogdu, Guney, 2007).

Unlike OK, where the mean μ is assumed constant over the entire region of study, UK assumes that the mean $\mu(x_i)$ is dependent on the spatial location (Kiš, 2016).

Also for the UK, in this study different semi-variogram models are used.

3.7 Accuracy Evaluation

To assess the accuracy of the results, Cross Validation (CV) is carried out. CV is a statistical validation technique to assess the performs of an interpolation algorithm (Alcaras et al., 2022). There are different methods available in literature for CV application (Browne, 2000; Falchi et al., 2018).
In this case, leave-one-out (CV-LOO) method is adopted. It consists in removing a point from the starting series and calculating the height/depth in the removed point using the height/depth of the other points and applying the same interpolation algorithm you want to test (Fasshauer, Zhang, 2007).

Therefore, as many heights are calculated as there are points. Finally, the difference between the single measured point and the predicted (calculated) value is checked, analysing the statistical values of these residuals, such as mean, standard deviation, minimum, maximum and Root Mean Square Error (RMSE) (Li, 1988; Aguilar et al., 2005).
RMSE is calculated in accordance with the formula:

$$RMSE = \sqrt{\frac{\sum_{i=1}^{n}(Z_i(x,y) - Z_i'(x,y))^2}{N}} \quad (8)$$

Where: N is the number of the depth points.
Z_i (x,y) is the measured depth at the location i(x, y);
$Z_i'(x,y)$ is the interpolated depth at the same location i(x, y).

4. RESULTS AND DISCUSSION

In this study, we applied the different interpolation methods previously described producing totally twenty-three DDMs.
Considering that the bathymetric dataset is derived from the ENC of the Port of Naples in scale 1:10,000, we choice the cell at 5 m for all generated models. This is in accordance with the study "finding the right pixel" proposed by Hengl (Hengl, 2006).

Optimization is performed for all the models obtained with the different interpolation methods; particularly, we use the option supplied by Geostatistical Analyst that allows the automatic parameter setting to optimize the results reducing the CV residuals. In Table 1 the statistics of the residuals supplied by the CV-LOO are reported.

For deterministic methods, the range of the minimum values is between -56.139 m for GPI-1 and -16.790 m for LPI-4. For stochastic methods, the minimum value goes from -19.603 m for OK-ES to -11.195 m for OK-KBS.
For deterministic methods, the maximum value ranges from 19.724 m for RBF-MF and 43.971 m for GPI-1. For stochastic methods, the range of maximum value goes from 15.584 m for OK-JBS to 19.720 m for OK-ES.

For deterministic methods, the mean value is between -0.241 m for RBF-IMF and 0.653 m for LPI-2. For the stochastic methods, the range of the mean goes from -0.026 m for OK-S and OK-JBS, to 0.013 m for UK-S and UK-KBS.
For the deterministic methods, the range of the standard deviation values is between 1.656 m for RBF-MF and 18.720 m for GPI-1. For the stochastic methods, standard deviation values go from 1.384 m for OK-S, to 2.472 m for UK-SS and UK-KBS.

About RMSE values, for the deterministic methods the range is between 1.656 m for RBF-MF and 18.720 m for GPI-1. In the end, for the stochastic methods, RMSE goes from 1.384 m for OK-S, to 2.472 m for UK-S and UK-KBS).

Therefore, analysing all RMSE values reported in Table 1, for both deterministic and stochastic methods, we see that the best performing method is OK-S. Since the performance of each method is related to the specificity of the analysed situation, we cannot say in absolute that OK-S is the best algorithm to interpolate bathymetric data derived from an ENC. On the other side, the results confirm the ability of the stochastic approaches compared to deterministic approaches for better modelling the seabed.

Interpolat. Method	Statistics of the residuals				
	Min (m)	Max (m)	Mean (m)	St. Dev (m)	RMSE (m)
IDW	-24.290	20.000	-0.071	2.371	2.372
GPI-1	-56.139	43.971	0.000	18.720	18.720
GPI-2	-27.287	40.018	0.000	9.331	9.331
GPI-3	-25.390	36.707	0.000	7.859	7.859
GPI-4	-24.566	34.390	0.000	7.250	7.250
GPI-5	-48.730	33.447	0.000	6.458	6.458
LPI-1	-19.956	23.472	0.241	4.503	4.509
LPI-2	-17.565	20.421	0.653	4.593	4.639
LPI-3	-18.444	21.937	0.133	4.036	4.038
LPI-4	-16.790	22.345	0.021	3.317	3.317
LPI-5	-17.790	22.752	0.052	3.787	3.788
RBF-CRS	-19.818	19.892	-0.096	2.053	2.055
RBF-SWT	-19.708	19.877	-0.093	2.035	2.038
RBF-MF	-19.605	19.724	-0.002	1.656	1.656
RBF-IMF	-24.467	22.667	-0.241	2.884	2.894
OK-S	-11.218	15.687	-0.026	1.384	1.384
OK-JBS	-11.490	15.584	-0.026	1.388	1.388
OK-KBS	-11.195	15.762	-0.025	1.386	1.386

OK-ES	-19.603	19.720	0.010	1.543	1.543
UK-S	-14.704	19.411	0.013	2.472	2.472
UK-JBS	-13.569	18.641	0.011	2.285	2.285
UK-KBS	-14.788	19.422	0.013	2.472	2.472
UK-ES	-13.754	18.890	0.010	2.468	2.468

Table 1. Statistics of the residuals supplied by Cross Validation for all methods applied.

Figure 3 shows the worst model obtained using deterministic methods, i.e. GPI-1. Figure 4 shows the best performing model among those resulting from the application of a deterministic method, i.e. RBF-MF. Figure 5 shows the best performing model among those resulting from the application of a stochastic method, i.e OK-S.

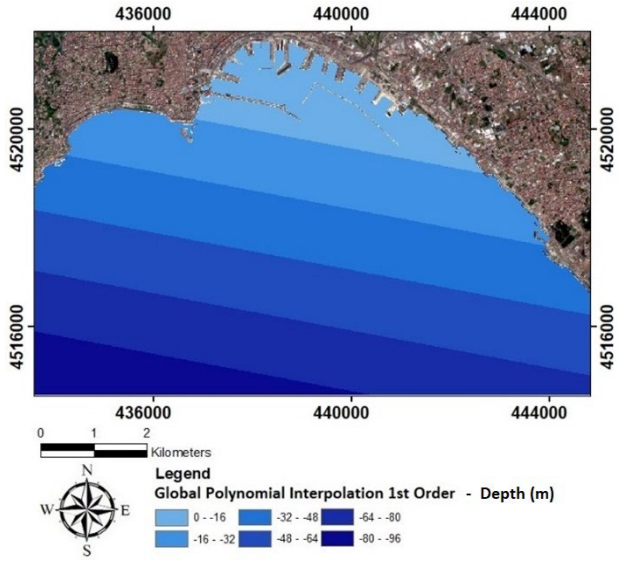

Figure 3. 2D visualization of the bathymetric model resulting from Global Polynomial Interpolation - 1st order interpolation method.

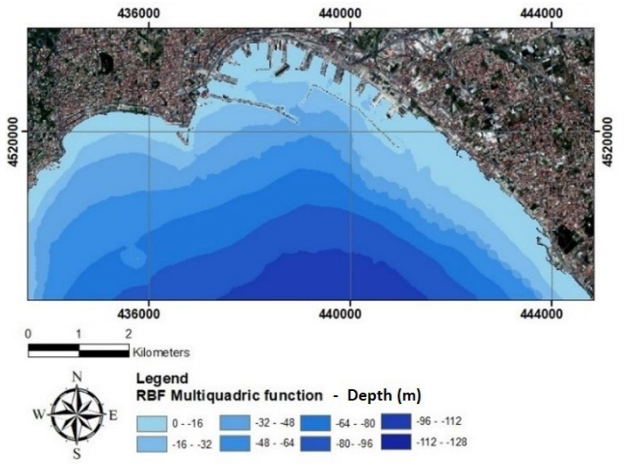

Figure 4. 2D visualization of the bathymetric model resulting from Radial Basis Function Multiquadratic interpolation method.

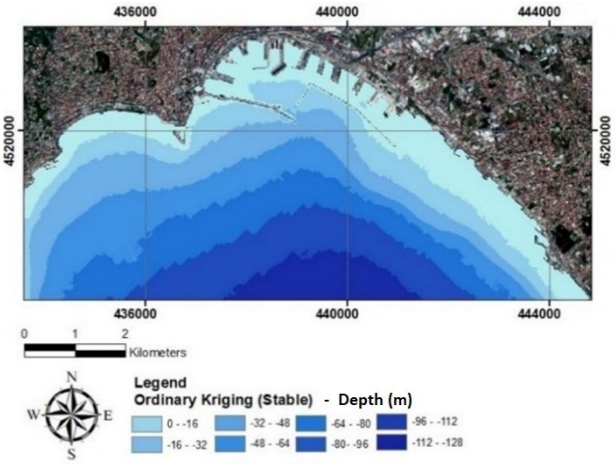

Figure 5. 2D visualization of the bathymetric model resulting from Ordinary Kriging interpolation method based on the application of Stable Semi-variogram Model.

5. CONCLUSION

This study illustrates the performance of spatial interpolation methods to produce 3D bathymetric models from an initial dataset obtained by ENC and containing 16,853 depth points selected from isolines and soundings. Specifically, we consider deterministic as well as stochastic approaches and use CV–LOO to analyse the performance of twenty-three methods.

About the deterministic methods, RBF-M allows the best performing model, observable from the RMSE values; GPI-1 presents the worst results, as it was possible to expect, since this algorithm turns out an inclined plane interpolating the analysed points.

For the stochastic methods, OK-S allows the best performing model; UK-S and UK-KBS present the worst results.
Ultimately, comparing all the interpolation methods used, and analysing the RMSE values, we can say that the best performing method for the considered dataset is OK-S.

The results obtained remarks the efficiency and the high performance of the Kriging interpolators. Furthermore, it can be noted that the choice of the mathematical model of the semi-variogram has a considerable influence.

About the future developments of this work, further studies will be focused on the relationship between interpolation methods and seafloor morphology as well as point density and model accuracy.

REFERENCES

Aguilar F. J., Agüera F., Aguilar M. A., Carvajal F., 2005. Effects of terrain morphology, sampling density, and interpolation methods on grid DEM accuracy. *Photogrammetric Engineering & Remote Sensing,* 71(7), 805-816.

Ajvazi B., Czimber K., 2019. A comparative analysis of different DEM interpolation methods in GIS: case study of Rahovec, Kosovo. *Geodesy and cartography*, 45(1), 43-48.

Alcaras E., Parente C., Vallario A., 2021. From electronic navigational chart data to sea-bottom models: Kriging

approaches for the Bay of Pozzuoli. *ACTA IMEKO*, 10(4), 36-45.

Alcaras E., Amoroso P.P., Parente C., 2022. The Influence of Interpolated Point Location and Density on 3D Bathymetric Models Generated by Kriging Methods: An Application on the Giglio Island Seabed (Italy). *Geosciences 2022*, 12, 62.

Arun P. V., 2013. A comparative analysis of different DEM interpolation methods. *The Egyptian Journal of Remote Sensing and Space Science*, 16(2), 133-139.

Baxter B., 2010, The interpolation theory of radial basis functions. arXiv preprint arXiv:1006.2443.

Brčić D., Kos S., Žuškin S., 2015. Navigation with ECDIS: Choosing the proper secondary positioning source. *TransNav: International Journal on Marine Navigation and Safety of Sea Transportation*, 9(3).

Browne M. W., 2000. Cross-validation methods. Journal of mathematical psychology 2000, 44(1), 108-132.

Buhmann M. D., 2000. Radial basis functions. *Acta numerica*, 9, 1-38.

Dabrowski P. S., Specht C., Specht M., Makar A., 2021. Three-Dimensional Thematic Map Imaging of the Yacht Port on the Example of the Polish National Sailing Centre Marina in Gdańsk. *Applied Sciences*, 11(15), 7016.

De Smith M. J., Goodchild M. F., Longley P., 2007. Geospatial analysis: a comprehensive guide to principles, techniques and software tools. Troubador publishing ltd, Leichester (UK).

Eberly S., Swall J., Holland D., Cox B., Baldridge E., 2004. Developing Spatially Interpolated Surfaces and Estimating Uncertainty, U.S. Environmental Protection Agency Office of Air Quality Planning and Standards Emissions, Monitoring and Analysis Division Research Triangle Park, NC 27711, November 2004.

Falchi U., Parente C., Prezioso G., 2018. Global geoid adjustment on local area for GIS applications using GNSS permanent station coordinates. *Geodesy and Cartography*, 44(3), 80-88.

Fasshauer G. E., Zhang, J. G., 2007. On choosing "optimal" shape parameters for RBF approximation. *Numerical Algorithms*, 45(1), 345-368.

Frederik M. C., Adhitama R., Hananto N. D., Sahabuddin S., Irfan M., Moefti O., Putra D. M., Riyalda B. F., 2019. First results of a bathymetric survey of Palu Bay, Central Sulawesi, Indonesia following the Tsunamigenic Earthquake of 28 September 2018. *Pure and Applied Geophysics*, 176(8), 3277-3290.

Gundogdu K. S., Guney, I., 2007. Spatial analyses of groundwater levels using universal kriging. Journal of earth system science, 116(1), 49-55.

Hare R., Eakins B., & Amante, C. J. T. I. H. R., 2011. Modelling bathymetric uncertainty. *The International Hydrographic Review,* 2011(6).

Hengl T., 2006. Finding the right pixel size. *Computers & geosciences*, 32(9), 1283-1298.

Infantes E., Terrados J., Orfila A., Canellas B., Alvarez-Ellacuria, A., 2009. Wave energy and the upper depth limit distribution of Posidonia oceanica. *Botanica Marina*, 52(5).

Johnston K., Ver Hoef J. M., Krivoruchko K., Lucas N., 2001. Using ArcGIS geostatistical analyst (Vol. 380). ESRI, Redlands, CA, USA.

Kiš M. I., 2016. Comparison of Ordinary and Universal Kriging interpolation techniques on a depth variable (a case of linear spatial trend), case study of the Šandrovac Field. *Rudarsko-geološko-naftni zbornik*, 31(2), 41-58.

Koutroulis A. G., Vrohidou A. E. K., Tsanis I. K., 2011. Spatiotemporal characteristics of meteorological drought for the island of Crete. *Journal of Hydrometeorology*, 12(2), 206-226.

Kristić M., Žuškin S., Brčić D., Valčić S., 2020. Zone of confidence impact on cross track limit determination in ECDIS passage planning. *J. of Marine Science and Eng.,* 8(8), 566.

Krivoruchko K., 2011. Spatial statistical data analysis for GIS users, 928, Redlands: Esri Press.

Ladage S., Gaedicke C., Barckhausen U., Heyde I., Weinrebe W., Flueh, E. R., Heyde I., Krabbenhoft A., Kopp H., Fajar S., Djajadihardja, Y., 2006. Bathymetric survey images structure off Sumatra. *Eos, Transactions American Geophysical Union*, 87(17), 165-168.

Li J., Heap A. D., 2014. Spatial interpolation methods applied in the environmental sciences: A review. *Environmental Modelling & Software*, 53, 173-189.

Li Z., 1988. On the measure of digital terrain model accuracy, *The Photogrammetric Record*, 12(72), 873-877.

Luo W., Taylor M. C., Parker S. R., 2008. A comparison of spatial interpolation methods to estimate continuous wind speed surfaces using irregularly distributed data from England and Wales, International *Journal of Climatology: A Journal of the Royal Meteorological Society*, 28(7), 947-959, 2008.

Mitas L., Mitasova H., 1999. Spatial interpolation. Geographical information systems: principles, techniques, management and applications, 1(2).

Oliver M., Webster R., Gerrard J., 1989. Geostatistics in physical geography. Part I: theory. Transactions of the Institute of British Geographers, 259-269.

Parente C., Vallario A., 2019. Interpolation of Single Beam Echo Sounder Data for 3D Bathymetric Model. *International Journal of Advanced Computer Science and Applications*, 10(10)., 6-13.

Plets R., Quinn R., Forsythe W., Westley K., Bell T., Benetti S., McGrath F., Robinson R., 2011. Using multibeam echo-sounder data to identify shipwreck sites: Archaeological assessment of the Joint Irish Bathymetric Survey data. *International Journal of Nautical Archaeology*, 40(1), 87-98.

Setianto A., Triandini, T., 2013. Comparison of kriging and inverse distance weighted (IDW) interpolation methods in lineament extraction and analysis. *J. of Applied Geology*, 5(1).

Walvoort D. J., de Gruijter J. J., 2001. Compositional kriging: a spatial interpolation method for compositional data. *Mathematical Geology*, 33(8), 951-966.

Wang S., Huang G. H., Lin Q. G., Li Z., Zhang,H., Fan Y. R., 2014. Comparison of interpolation methods for estimating spatial distribution of precipitation in Ontario, Canada. *International Journal of Climatology*, 34(14), 3745-3751.

Weatherall P., Marks K. M., Jakobsson M., Schmitt T., Tani S., Arndt J. E., Rovere M., Chayes D., Ferrini V., Wigley R., 2015. A new digital bathymetric model of the world's oceans. *Earth and space Science*, 2(8), 331-345.

Webster R., Oliver, M. A., 2007. Geostatistics for environmental scientists 2007. John Wiley & Sons, Chichester, England.

Wlodarczyk-Sielicka M., Stateczny A., 2016. Clustering bathymetric data for electronic navigational charts. *The Journal of Navigation*, 69(5), 1143-1153.

Zimmerman D. L., Zimmerman M. B., 1991. A comparison of spatial semivariogram estimators and corresponding ordinary kriging predictors. *Technometrics*, 33(1), 77-91.